To be submitted to the *Astronomical Journal*.
Preprint date: 1993 October 21

Near–infrared Continuum and 3.3 μm PAH Imaging of the Starburst Ring in the Type 1 Seyfert Galaxy NGC 7469

J. M. Mazzarella
Infrared Processing & Analysis Center, MS 100-22, California Institute of Technology,
Jet Propulsion laboratory, Pasadena, CA 91125
Electronic mail: mazz@ipac.caltech.edu

G. M. Voit
Theoretical Astrophysics, California Institute of Technology;
Department of Physics and Astronomy, The Johns Hopkins University, Baltimore, MD 21218
Electronic mail: voit@pha.jhu.edu

B. T. Soifer and K. Matthews
Palomar Observatory, MS 320-47, California. Institute of Technology, Pasadena, CA 91125;
Electronic mail: bts@mop.caltech.edu; kym@tacos.caltech.edu

J. R. Graham
Department of Astronomy, University of California, Berkeley, CA 94720
Electronic mail: jrg@graham.berkeley.edu

L. Armus and D. Shupe
Palomar Observatory, MS 320-47, California, Institute of Technology, Pasadena, CA 91125
Electronic mail: lee@mop.caltech.edu; shupe@mop.caltech.edu

ABSTRACT

nigh resolution near-infrared images of the type 1 Seyfert galaxy NGC 7469 have been obtained to probe its dusty nuclear environment. Direct J, 11, & K images are relatively featureless, but residual images created by subtracting a smooth model based on best-fitting elliptical isophotes reveal a tight inner spiral whose high surface-brightness portions correspond to a previously detected 3" (1 kpc) diameter ring of radio continuum emission. The inner infrared spiral arms extend ≈ 4" NW and SE from the nucleus, and the NW arm joins up with large-scale spiral structure visible in the R band. The residual images also show a bar-like structure aligned with the brightest infrared/radio hotspots at PA≈50°. Three infrared hotspots arc detected which align remarkably well with the 6 cm radio peaks. The near-infrared ring and the hotspots arc visible in the residual images, and in a high-resolution direct K-band image restored to an effective resolution of 0.″65 FWHM using the Richardson-liucy algorithm. The infrared hotspots have luminosities of $\nu L_\nu(2.2\mu m) \approx 10^8 L_\odot$ ($M_K \approx$ -16 mag), suggesting they are either giant HII regions or individual supernovae. The two brightest regions may be associated with enhanced star formation triggered by orbit crowding of gas where spiral arms emerge from an inner bar. Narrow- band ($\Delta\lambda/\lambda \sim 1$ .5%) imaging in the 3.28 μm dust emission feature and surrounding continuum confirms the 3" diameter 3.28 μm emission region detected previously using multi-aperture photometry. The extended }'All emission is slightly elongated and aligned with published [0 III] line emission and 12.5 μm continuum emission, apparently tracing the starburst. The overall circular symmetry of the }'All emission indicates that few X-rays from the AGN emerge in the plane of the sky. The presence of ≈ 25% of the total 3.28 μm PAH emission within R < 1" demonstrates that a starburst within the central fcw hundred parsecs must supply a significant fraction of the infrared continuum from the nucleus, and there is apparently sufficient shielding material between the starburst and the AGN to preserve the PAHs along our line of sight to the nucleus.

1. Introduction

NGC 7469 (= Arp 298 = UGC 12332= Mrk 1514) is a well- known type 1 Seyfert galaxy which was identified as a bright far-infrared source by the Infrared Astronomical Satellite (e.g., Soifer et al. 1987). Its high infrared luminosity, $L_{ir} \approx 3.4 \times 10^{11} L_{\odot}$, approaches that of quasars, and the high infrared-to-blue luminosity ratio, $L_{ir}/L_b = 15$, implies that dust reprocesses the bulk of its luminosity into the infrared, The nucleus has been observed to vary rapidly at many wavelengths, and it is one of the fcw luminous Seyfert galaxies showing direct evidence for active circumnuclear star formation. NGC 7469 was the first Seyfert galaxy in which the 8.7 and 11.3 μm dust emission features were observed (Aitken, Roche, & Phillips 1981); these features arc common in starburst galaxies, but rare in Seyferts. Multiaperture single- channel photometry showed that $\approx$80% of the luminosity in the 3,3 μm dust emission feature emerges from a region 1- 3" (0.3-1 kpc) from the nucleus (Cutri et al. 1984). (At a distance of 68.3 Mpc, assuming 11_0=75 km s-' Mpc^{-1}, 1" corresponds to 330 pt.) The high apparent dust temperature (> 300 K) at $\sim$1 kpc from the central source led Cutri et al. to conclude that an extended starburst, rather than the Seyfert nucleus, heats the dust. CO (J=1→ O) mapping shows that NGC 7469 has $\approx$ 2 x 10^{10} $M_{\odot}$ of molecular gas within 2,5 kpc of its nucleus, an ample concentration of the dense material needed to fuel a starburst (Meixner et al. 1990).

Recent 6 cm continuum and optical emission-line images have begun to resolve the structure of the circumnuclear star- forming region in NGC 7469 (Wilson et al. 1991). While [OIII] and Hα+[N 11] maps show few details, the 6 cm continuum image suggests that a broken ring $\approx$3" (1 kpc) in diameter encircles the nucleus. Drawing analogy to NGC 1068, in which a circumnuclear ring of molecular gas $\sim$ 3 kpc in diameter (Planesas, Scoville, & Myers 1991) is associated with a small-scale stellar bar found at 2 μm (Scoville et al. 1988), Wilson et al. noted that near- infrared imaging of NGC 7469 might also reveal a stellar bar and possibly individual supernovae associated with the starburst ring.

The infrared emission features at 3.3, 6.2, 7.7, 8.7 and 11,3 μm, first seen in spectra of Galactic sources (e.g., Sellgren 1981, Soifer, Russell, & Merrill 1976), have been ascribed to polycyclic aromatic hydrocarbons (PAHs) transiently heated by single UV photons (e.g., Puget & Luget 1989). Although the agreement between laboratory spectra of PAHs and the interstellar emission features is not yet entirely satisfactory, wc will refer to the emitters of these features as PAHs. Single aperture observations encompassing $\approx$2" radii have detected PAH features in $\gtrsim$90% of observed starburst galaxies, but $\lesssim$10% of Seyfert galaxies have such emission (Roche et al. 1990). This dichotomy led Aitken & Roche (1 985) to suggest that extreme ultraviolet (EUV) photons emerging from AGNs efficiently destroy these small grains. When PAHs have been detected in Seyfert galaxies, the mission appears to be extended and is usually seen only in large apertures, suggesting that PAHs tend to lie outside a radius of $\approx$ 500 pc in a circumnuclear starburst (e.g., Cutri et al. 1984, Desert & Dennefeld 1988). However, these studies relied on single channel measurements, and the detailed spatial distribution of the PAH emission in NGC 7469 and other

Seyfert galaxies has remained unknown.

Photo-dissociation and Coulomb explosion via absorption of energetic EUV/X-ray photons are likely to destroy PAHs near Seyfert nuclei (Voit 1992). Although these processes can destroy PAHs within ~ 1 kpc of a typical Seyfert nucleus, PAHs can survive in directions along which a sufficient column density of X-ray absorbing material shields them from the nucleus. Regions of I'AH emission in active galaxies therefore trace those locales where the relatively soft UV radiation field originating from hot, massive stars heats a dusty medium shielded from the AGN. Conversely, its absence indicates either a lack of shielding or a lack of stellar heating sources. imaging in the PAH features thus provides a potentially powerful tool to investigate the angular distribution of absorbing material surrounding the nucleus and the spatial distribution of star-formation activity in the dusty circumnuclear environments of AGNs.

We report the results of new high resolution near- infrared imaging of NGC 7469. In §2 the observations and data reduction are described. Section 3 presents broad-band images showing that the starburst ring is part of a tightly wound inner spiral with infrared hotspots that correspond to peaks in the 6 cm continuum image. Narrow- band imaging in the redshifted 3.28 μm I'AH feature and surrounding continuum illustrate the extended distribution of hot dust in the star- forming region surrounding the Seyfert nucleus. The results are discussed in §4.

2. Observations and Data Reduction

Near- infrared images of NGC 7469 were obtained with the Cassegrain infrared camera on the 5 m 11 ale telescope of Palomar Observatory. The camera's 58x62 element InSb array, at 0.″31 pixel^{-1}, results in a field of 18″ × 19". Data were obtained through J (1 .27 pm), 11 (1 .65 μm), and K (2.20 μm) filters on 1992 July 17 UT. Observations at J, 11, & K, performed by nodding the telescope between the galaxy and regions of adjacent Mank sky, yielded many short exposures of 10 s to 50 s duration and cumulative on-source integration times of 320 s at J, 200 s at 11, and 140 s at K. The point-spread function determined from measurements of the unresolved Seyfert nucleus indicated an average seeing at 2.2 μm of 0.″8 FWHM, with a range of 0.″73 to 1.″02 FWHM.

The 3.28 μm PAH feature was imaged on 1992 July 17 and July 18 UT using a circular variable filter (CVF) with a band pass of 0.05 μm ($\Delta\lambda/\lambda \sim 1.5\%$). Images were centered on 3.33 μm (the redshifted peak of the 3.28 μm feature), 3.42 μm (the redward shoulder of the feature, see e.g., Geballe et al. 1985), and 3.20 μm (continuum). Each exposure comprised 200 integrations of 0.4 s duration taken while chopping the secondary between the source and reference sky regions, The CVF plus atmospheric transmission was calibrated using observations of SAO 127810 (a type F5V star) taken close in time and within 0.1 airmass of the galaxy integrations. The average seeing of 0.″8 at 3.3 μm on both nights justified combining the CVF images to produce coadded images at 3.33 μm, 3.42 μm, and 3.20 μm.

All images were reduced by first correcting for non-linear response, and then subtracting

the appropriate median sky frame from each object frame. Flat-field images of the night sky were created by applying an iterative sigma clipping algorithm to a large number of reference sky images, subtracting a high signal- to noise dark frame, and then normalizing to unity at the array center. Flux calibration was based on observations of infrared stand ard stars (Elias et al. 1982). The CVF images required additional processing, including atn~osphcrc/filter transmission corrections derived from the reference star observations. All images were aligned by forcing the centroids of the nucleus to coincide using a bicubic splint interpolation algorithm.

3. Results

Figures 1a, 1 c, & 1 c show the direct J, 11, and K images. Differences between the position angles and ellipticities of the inner and outer isophotes, as well as slight deviations from ellipticity, indicate that underlying non-axisymmetric structures could be unveiled by subtracting the bright Seyfert nucleus and the underlying intensity gradient of the galaxy, in order to model the smooth, axisymmetric bulge, disk, and nuclear components, models consisting of best-fitting elliptical isophotes were subtracted from the direct images at J, 11, and K. The outer isophotes beyond a radius of 5" were fitted first, allowing ellipticity and position angle to change with radius while keeping the isophotes centered on the nucleus. The major axes of the outer ellipses, which correspond to the large-scale stellar disk of the galaxy, mai nt ained a st able posit ion angle of 11 8°±4° and an ellipticity of 0.20+- 0.07. In order to study deviations from axisymmetry in the disk, the ellipse fitting was then continued in the inner region at a fixed position angle of 11 8°; the ellipticity was allowed to vary in order to track contributions from the bulge and nucleus components. The position angle of the stellar disk derived from surface photometry at J, 11, and K agrees well with the value of 1210 obtained from optical imaging (Burbidge, Burbidge, & Prendergast 1963). The fitting was also performed allowing the position angle to vary with radius, and this had negligible effect on the resulting residual image. The residual, model-subtracted images arc shown in Fig. 1 next to the corresponding direct images.

It is also worthwhile to examine structures in the *direct* images by improving the effective resolution, with no model-dcpcndcnt galaxy background subtraction. The direct K-band image was restored using the Richardson- Lucy method. This algorithm restores (super-rcso]vcs) an image by iteratively convolving a mode] image with the point-spread function and comparing it with the previous model. The single 60 s K-band integration with the highest resolution (0.″73) was iteratively restored to a convergence criterion of $\chi^2 = 1$, which gave an effective resolution of 0.″65 FWHM, measured for the nucleus. Figure 2 shows gray-sc.ale, contour, and radial profile plots of the K-band image after Richardson-Lucy restoration.

We investigated whether the structure present in the residual images of NGC 7469 might be due to faint irregularities in the point-spread function (PSF). Close examination of bright standard-star images showed no such structure with corresponding intensity levels and morphologies in any band. The structures in the processed images of NGC 7469 arc therefore

intrinsic to the galaxy, not artifacts of low level structure in the PSF. The peak located 1".5 SW of the nucleus and the faintest spiral emission represent 39% (36%) and 14% (13%) residuals above the surrounding galaxy background at K (J), respectively, but are difficult to see in the direct images because of their low contrast against the steep gradient in the underlying galaxy and the bright emission from the nuclear point source.

Photometry performed on the *direct* images within circular apertures centered on the nucleus gave fluxes uncertain to 5% - 7%. The inner spiral and the hotspots were measured from the residual images; the relative uncertainties in these measurements are estimated to be $\approx 30\%$ based on the internal consistency of the values obtained using slight variations in the smooth model images and in the boundaries used to define the knots. Although there are large uncertainties in the fluxes estimated from the residual images, these estimates still provide useful constraints on the nature of the emitting regions. The photometric measurements are given in 'J'able 1.

Figure 3 shows the CVF images taken on and off the redshifted 3.3 μm dust emission feature, as well as the resulting continuum-subtracted image. Tables 1 & 2 report the photometry from integrating the CVF images within circular apertures.

4. Discussion

4.1. 'J'he Inner Near-Infrared Spiral

The direct images in Fig. 1 show isophote twisting between 1" - 4" from the center, signifying a transition between the galactic bulge and a possible bar component at small radii and the exponential disk which dominates the emission at large radii. After subtraction of the smooth underlying light distribution, the residual images shown in Fig. 1 reveal that the starburst "{ring" is the high surface-brightness portion of a tight inner spiral with an inner radius of $\approx 1".5$ (0.5 kpc). The arms appear to be attached to a bar-like structure at PA$\approx 50°$, and they can be traced in the J, 11, and K-band images out to 4" from the nucleus in the NW and SE directions. Although one third the physics] size, this structure may be analogous to the $\sim 30"$ (3 kpc) diameter inner spiral in the nearby type 2 Seyfert galaxy NGC 1068 detected at optical and infrared wavelengths (Telesco et al. 1984) and in molecular gas (Planesas, Scoville, & Myers 1991).

Fig. 4 illustrates the orientation of the small-scale infrared structure in relation to the high-resolution 6 cm radio continuum (cf., Wilson et al. 1991) and the large-sc,alc spiral structure in an R-band image obtained with the University of Hawaii's \$8 inch telescope. The direct R-band image in Fig. 4c shows the bright northern arm which joins up with the center of the galaxy near a foreground star located 12" NW of the nucleus. This northern spiral arm is also visible in an Hα/[O 111] ratio image (De Robertis & Pogge 1986), Fig. 4b presents the central 30" region of a residual R.-band image after subtraction of a smooth model to enhance visibility of the spiral structure. The superposed contours show clearly that the inner near- infrared arm on the NW

side of the galaxy is also visible in the R-band and is merely the beginning of a spiral that winds around the SE side of the galaxy and joins with the outer spiral structure.

Wilson et al. (1991) suggested that an optically obscured stellar bar might drive the dynamics of the broken ring structure observed in the 6 cm radio continuum image of NGC 7469. Theoretical models predict that rings in galaxies, thought to be formed by Linblad resonances between stellar orbits and the pattern speed of an oval gravitational distortion (a stellar bar), can force disk gas inward and provide fuel for an AGN (e.g., Simkin, Su, & Schwarz 1980, Schwarz 1984, Matsuda et al. 1987, Shlosman, Frank, & Begelman 1989), Observations showing that rings in galaxies arc typically associated with stellar bars support this hypothesis (e.g., Huts. 1986, Kennicutt 1993). The *direct* near--infrared images at J, 11, & K fail to show compelling evidence for the putative stellar bar at the resolution limit of the present data, However, the bright Seyfert nucleus can easily overwhelm underlying structure in the stellar distribution near the center of the galaxy. The J, H, and K-band *residual* images indeed show an oval bar-like structure along PA≈50° on the scale of the spiral ring (c, f., Figs. 1b, Id, If & 4a), The two brightest infrared/radio features lie where the spiral arms emerge from this apparent bar. Hotspots are often observed on the ends of stellar bars (e.g., Kennicutt 1993), and numerical simulations indicate that star formation can be cnha.need by orbit crowding of interstellar gas clouds where the spiral arms connect with a bar or ring (see e.g., Kenney & Lord 1991, Roberts, Huntley, & van Albada 1979). Infrared imaging with higher resolution is required to confirm the nature of the bar-like structure present in the current residual images.

4.2. The Nature of the Infrared/Radio Hotspots

A major result of our high- resolution near- infrared imaging of the nuclear region of NGC 7469 is the detection of three infrared hotspots which correspond spatially to compact radio sources (c. f., Fig. 4a). As discussed in §3, the current data permit only rough flux and color estimates; however, these measurements hc]p constrain the nature of the hotspots. The most likely candidates for the infrared emission sources arc supernovae or supernova remnants, giant 11 II regions, and clusters of red supergiant stars.

The absolute K-band magnitudes of the three hotspots located SW, NW, & NE of the nucleus of NGC 7469 (cf., Fig. 2b & Fig. 4a) are $-16 \lesssim M_K \lesssim -15$, and their observed near- infrared colors are J-H≈0.9 mag and H-K≈0.7 msg. Assuming that the reddening correction derived from nuclear near-infrared spectroscopy, E(B – V) = 0.52 (Osterbrock, Tran, & Veilleux 1992), applies to the starburst spiral/ring region, and adopting the reddening curve of Mathis (1990), wc estimate intrinsic colors of J – H ≈ 0.7 mag and H – K ≈ 0.6 msg. The luminosities of the hotspots arc comparable to individual supernovae observed less than 200 days after the explosion (e.g., Graham 1985). For comparison, infrared hotspot "A" in the starburst galaxy NGC 253 has $M_K \approx -14$ mag (Forbes, Ward, & DePoy 1991); this is 1–2 mag fainter than the hotspots in NGC 7469, more consistent with a faded type 11 supernova ($t \gtrsim 200$ days) or a supernova remnant. The J – H and

11 – K colors do not match those of observed supernovae in any particular phase (cf., Elias et al. 1985, Dwek 1983). However, the colors do not rule out ndividual supernovae embedded in a dense shell with strong thermal dust emission (e.g., Dwek et al. 1983), The presence of *three* infrared/radio hotspots argues against the supernova hypothesis. Even in a galaxy as luminous as NGC 7469, with an expected supernovae rate of 0.5--1 yr^{-1} (e.g., Wright et al. 1988, van Buren & Greenhouse 1993), wc would not expect to observe two or three supernovae simultaneously in the same region of the galaxy. Proof that one or more of the infrared/radio hot spots are supernovae will require follow-up observations to demonstrate variability. 'l'he physical sizes of the individual hotspots ($D \lesssim 0.3$ kpc) arc comparable to the starburst regions in M 82 and NGC 253, and the infrared luminosity of each feat ure could also be explained by a fcw supernova remn ants spread thoughout these large regions.

Another possibility is that the hotspots represent large complexes of massive star formation. The near-infrared emission from giant H 1 I regions may have a number of significant components, including gaseous emission (recombination lines, free-free, and free-bound continua.), photospheric emission from the hot ionizing stars, a cluster of cool red giant and supergiant stars which evolve rapidly in the starburst, and thermal emission from warm dust. Campbell & Terlevich (1984) have modeled these emission sources to interpret observations of 14 giant H 11 regions. Although it is not possible to determine the exact composition from the present data, the K-band luminosities and extinction-corrected J – 11 and H – K color intimates for the hotspots in NGC **7469** arc consistent with emission dominated by red supergiant stars (~80%), with small contributions from gaseous emission (~10%) and warm dust (~10%). Assuming $M_K = -11.5$ mag for a red supergiant (Campbell & Terlevich), 25- 150 such stars would be required to explain the K-band luminosity of the hotspots detected in NGC 7469. Although these arc luminous hotspots, 2-3 mag brighter than giant 11 11 regions in the spiral arms of M 101, they are comparable to the largest star-forming regions observed in NGC 5253 and in a number of blue dwarf galaxies; however, the most luminous 11 H regions observed by Campbell & Terlevich have projected physical diameters of 0.7 kpc to a fcw kpc (adjusted to $H_o = 75$ km $s^{-1} Mpc^{-1}$), which is somewhat larger than the hotspots in NGC 7469 ($D \sim 0.3$ kpc). The radio emission in the ring of NGC 7469 is also consistent with current star formation models (Wilson et al. 1991); the radio sources are likely due to synchrotrons emission from supernova remnants,

4.3. The 3.3 μm PAH Dust Emission

As reviewed in §1, NGC 7469 is onc of the few Seyfert galaxies in which I'All emission features have been detected. Using single-channel measurements, Cutri et al. 1984 showed that 80% of the 3.3 μm emission comes from an annular region between 1" < R < 3". The presence of this extended PA]] emission indicates that a relatively soft UV radiation field originates from hot, massive stars in regions shielded from the AGN. Since significant emission emerges from within a 2" diameter beam centered on the nucleus, the shielding material responsible for preserving the

PAHs must lie within a couple hundred parsecs of the nucleus, perhaps in the form of an obscuring torus of molecular gas in between the broad and narrow line regions (e.g. Krolik & Begelman 1986, 1988).

Unfortunately, the signal- to--noise of the present 3.28 μm CVF imaging data (Fig. 3) is insufficient to show any detailed morphology. The current data basically confirm the 3" diameter 3.28 μm mission region detected by Cutri et al. (1984). in addition, the data show that the extended I'All emission is slightly elongated and in rough alignment with the [0 III] emission and the axis of the two brightest radio hotspots (Wilson et al. 1991), and the extended 12.5 μm emission (Keto et al. 1992), all at PA$\approx$50°(c.f., Fig. 3). This general alignment is consistent with a starburst origin for the PAH emission, with in situ photoionization of the [0 111] and Hα line-emitting gas, The overall circular symmetry of the PAH emission suggests that little X-ray emission escapes the AGN in the plane of the sky, but instead emerges primarily along our line of sight. If transverse X-ray beams intersected the starburst region, they would create I'All emission gaps at certain position angles.

'l'able 2 summarizes the contributions of the 3.3 μm PAH emission in various annuli surrounding the nucleus, and measurements from Cutri et al. (1984) are listed for comparison, Within R< 1" PAH emission is still present, but it becomes substantially weaker relative to the I It continuum. in this region, both starburst radiation and AGN radiation, including emission from dust heated by the AGN, must contribute to the total infrared output, If wc assume that the PAH -to-continuum ratios from the starburst region remain similar within R < 1" ($f_{PAH}/f_{3.20\,\mu m} \approx 0.56$ and $f_{PAH}/f_K \approx 0.40$), our data allow us to estimate very crudely the relative contribution of the nuclear starburst to the flux from the unresolved nucleus. Since no PAH emission is expected from the AGN, the starburst contribution at 3.20 μm must be about 1/6 the total flux, and in the K band it must be about 1/3 the total flux. These numbers should be considered lower limits because wc have not accounted for a possible l'All-free starburst contribution from X-ray irradiated star-forming regions. This result agrees well with the AGN/stellar breakdown derived by deconvolving the disk, bulge, and nuclear profiles in images, Kotilainen ct al. (1992) find that, in a 3" diameter aperture, stars contribute 55% of the K band flux, 59% in H, and 66% in J. Also, Morris & Ward (1988) find substantial calcium infrared triplet absorption within 1".5 of the nucleus, indicating a significant stellar contribution to the continuum at 8500 Å.

5. Summary & Conclusions

Subtraction of smooth galaxy models derived from best-fitting elliptical isophotes (including the disk, bulge and nuclear light components) from direct J, 11, & K-band images of NGC 7469 show that the starburst ring (diameter $\approx$ 3", 1kpc) first detected in radio continuum emission (Wilson ct al. 1991) is part of a tight inner spiral. The arms of the infrared spiral extend= 4" NW and SE from the nucleus, and the northern arm joins with the large-scale spiral structure visible in the R band. Three distinct infrared hotspots align with components in the published 6 cm

radio continuum image. The near-infrared ring and the hotspots arc clearly visible in the residual images, and in a high-resolution *direct* K-band image restored to an effective resolution of 0.″65 FWHM using the Richardson-Lucy algorithm, The near-infrared luminosities and dereddened color estimates of the hotspots arc comparable to giant II 11 regions observed in other galaxies (Campbell & Terlevich 1984); the near-infrared emission from each feature can be attributed to $\sim$ 25 -- 150 red supergiant stars embedded in emitting gas and warm dust within star-forming regions. Possibly one or more of the hotspots represent individual dust- enshrouded supernovae observed less than one year after explosion; confirmation will require follow-up observations to demonstrate variability, The two brightest infrared/radio hotspots may be associated with clumps of enhanced star formation on the ends of a small-scale stellar bar oriented along PA$\approx$50°, where the spiral arms emerge. This phenomenon is observed in some galaxies with unobscured bars, and such structures appear in numerical simulations of the gas dynamics of barred spirals.

Narrow- band ($\Delta\lambda/\lambda \sim$1 .5%) imaging in the 3.28 μm dust emission feature and surrounding continuum shows PA]] emission throughout the inner starburst region of NGC 7469, confirming the 3“ diameter 3.28 μm emission region detected by Cutri et al. (1984) using multi-aperture photometry. The extended I'All emission is slightly elongated and roughly aligned along the axis of the two brightest infrared/radio hotspots, the [0 111] emission (Wilson et al. 1991), and the 12,5 μm mid-infrared emission (Keto ct al. 1992), at PA$\approx$50°. This general alignment is consistent with the hypothesis that the 3.28 μm emission is duc to small dust grains heated by UV radiation from vigorous star formation surrounding the nucleus, The overall circular symmetry of the PAH emission suggests that little of the X-ray emission from the AGN cuts across the starburst region in the plane of the sky, The X-rays probably escape along directions closer to our line of sight. Furthermore, the presence of PAH emission within R < 1” indicates that a shielded starburst within a few hundred parsecs of the nucleus supplies at least 1/3 of the nuclear K-band light and at least 1/6 of the nuclear continuum at 3,2 μm.

Wc thank A. Wilson and T. Helfer for sending their VLA image of NGC 7469, and Steve Lord and Dave van Buren for useful discussions. This work was supported by the Jet l'repulsion laboratory, California Institute of Technology, under a contract with the National Aeronautics and Space Administration (NASA). Additional support was provided by the NSF. Wc thank our night assistant at the 200 inch telescope, Juan Carrasco, and the entire staff of Palomar Observatory. The data were processed with IRAF and STSDAS. IRAF is produced by the National Optical Astronomy Observatories, which is operated by the Association of Universities for Research in Astronomy, Inc. (AURA) under cooperative agreement with the National Science Foundation. STSDAS is produced by the Space Telescope Science Institute. This research has also made use of the NASA/IPAC Extragalactic Database (NED) which is operated by the Jet l'repulsion laboratory, California Institute of '1'ethnology, under a contract with NASA.

Table 1. Near-Infrared Photometric Measurements of NGC 7469

Region	f_J (mag) (mJy)	f_H (mag) (mJy)	f_K (mag) (mJy)	$f_{3.20\mu m}$ (mJy)	$f_{3.33\mu m}$ (mJy)	f_{PAH} (mJy)	J – I I (mag)	H--K (mag)	M_K (mag)	log $(L_K/L_\odot)^c$
2“ Beam (Nucleus)?..	12.23	11.15	10,07	--	--	--	1.08	1.09	-20.8	10,1
	20.3	35.9	60.6	85.1	93.1	8.0	—	-		
4“ Beam[a]...	11.50	10.52	9.63	--	---	-	0.98	0.90	-21.3	10.3
	39.7	64.1	91.5	111.6	131.1	19,5	—	-	--	
5“ Beam[a]...	11.34	10.37	9.52	---	-	-	0.96	0.86	-21.4	10.3
	46.3	73.5	101.0	116.7	140.2	23.5	-	--	-	
6″ Beam[a]...	11.22	10.28	9.45	--	-	-	0.95	0.83	-21.5	10.4
	51.3	80.3	107.7	119.3	146.6	27.2	-		-	
8“ Beam[a]...	11.07	10$_s$1 5	9.36	“-		- --	0.93	0.79	-21.5	10.4
	59.1	90.7	117.3	123.7	153.3	29.5	--	-	-	
17″ Beam[a]..	10.73	9.86	9.17	--	-	-	0.91	0.69	-21.7	10.4
	80.6	118.3	139.2	--	-	-				
Ring/Spiral[b]’..	13.0	12.2	11.2	--	-	-	0.9	0.9	-19.7	9.5
	9.6	14.2	20.7	--	-	-	-			
SW Ridge[b]..	14.7	13.9	13.3	-	-	-	0.8	0.6	-17.6	8.6
	2.1	2.8	3.0	--	-	-	-			
Sw Hotspot[b]..	16.2	15.3	14.7				0.8	0.6	-16.2	8.0
	0.5	0.8	0.8	-	--	-	-	-	-	
NW Hotspot[b]..	17.5	16.6	15.8	--	-	-	0.9	0.8	-15.1	7.7
	0.2	0.3	0.3	-	-					
NE Hotspot[b]..	16.1	15.2	14.5	-	-	-	1.0	0,7	-16.4	8.2
	0.6	0.9	1.0	- -	-	-				

[a] 2--17″ Beams: integrated emission within the specified beam diameter centered on the nucleus of the *direct* images; the relative uncertainties in these measurements are 5% - 7%.

[b] These regions were measured from *residual* images after subtraction of smooth galaxy models derived from ellipse fitting; hence there are large uncertainties on the order of 30% in these flux densities and color magnitudes. Ring/Spiral: total emission in residual image, omitting the nucleus; SW Ridge: IR/radio ridge SW of nucleus; boundaries near 6th contour in Fig. 4a. SW hotspot: IR/radio hotspot 1″.5 SW of nucleus (peak in the ridge); boundaries near 7th contour in Fig. 4a.. NW hotspot: faint I]{/radio hotspot 1“5 NW of nucleus; boundaries near 5th contour in Fig. 4a, NE hotspot: infrared/radio hotspot 1″.5 NE of nucleus; boundaries between the 6th & 7th contours in Fig. 4a.

[c] The monochromatic luminosity at K (2.2 pm), defined as $L_K = 4\pi d^2 \nu f_\nu(K)$, where $L_\odot$ = 3.83 x 1 0^{33} erg s^{-1}.

'J'able 2: Distribution of the 3,3 μm PAH Emission in NGC 7469

Annulus Radii	From PAH Image				From Cutri et al. 1984[a]	
(arc sec)	f_{PAH} (mJy)	$\frac{f_{PAH}(annulus)}{f_{PAH}(total)}$	$\frac{f_{PAH}}{f_{3.20\mu m}}$	$\frac{f_{PAH}}{f_K}$	f_{PAH} (mJy)	$\frac{f_{PAH}(annulus)}{f_{PAH}(total)}$
0- 1...	8.0	0.28	0.09	0.13	4.6	0.21
1-2...	11.5	0.40	0.44	0.37	7.7	0.35
2-3...	7.7	0.27	0.99	0.48	10.5	0.48
3-4...	2,3	0.08	0.53	0.24	-	
1-3...	19.2	0.66	0.56	0.41	18.1	0.84
1-4..,	21.0	0.71	0.56	0,38	18.1	0.84
0-4 (Total). ,.	29.5	1.00	0.24	0.25	21.7[b]	1.00

[a] Flux densities were computed from the published luminosities using their assumed distance of *50.2 Mpc* for NGC *7469* and FWZI = 0.1μm for the 3.3 μm feature.

[b] The total flux density of the 3,3 μm feature was computed from the average of the luminosities measured in 5.″85 (5.0 ± 0.5 x 1071,.), 7.″8 (4.6 ± 1.0 x $10^7 L_\odot$), and 8.″7 (4.7 ± 0,7 x $10^7 L_\odot$) diameter beams by Cutri et al. 1984.

REFERENCES

Aitken, D. K., & Roche, P. F. 1985 MNRAS, 213,777

Aitken, D. K., Roche, P. F., & Phillips, M. M. 1981, MNRAS, 196, 1011'

Burbidge, E. M., Burbidge, G. R., & Prendergast, K. H. 1963, ApJ, 137, 1022

Buta, R. J. 1986, ApJS, 61, 609

Campbell, A. W., & Terlevich, R. 1984, MNRAS, 211, 15

Cutri, R. M., Rudy, R. J., Ricke, G. 11., Tokunaga, A. T., & Wilner, S. 1'.1984, ApJ, 280, 521

De Robertis, M. M., & Pogge, R.. W. 1986, AJ, 91, 1026

Desert, F. X., & Dennefeld, M. 1988, A&A, 206, 227

Dwek, E. 1983, ApJ, 274, 175

Dwek, E., et al. 1983, ApJ, 274, 168

Elias, J. H., Frogel, J. A., Matthews, K., & Neugebauer, G. 1982, AJ, 87, 1029

Elias, J. H., Frogel, J. A., Matthews, K., Neugebauer, G., & Persson 1985, ApJ, 296, 379

Forbes, D. A., Ward, M. J., & DePoy, D. 1,.1991, ApJ, 380, L63

Geballe, T. R.., Lacy, J. H., Persson, S. E., McGregor, P. J., & Soifer, B. T. 1985, ApJ, 292, 500

Graham, J. R. 1985, PhD thesis, University of London

Kennicutt, R. C., 1993, in Mass-Transfer Induced Activity in Galaxies, 1. Shlosman, Cambridge University Press, in press.

Kenney, J. D. P., & Lord, S. D. 1991, ApJ, 381, 118

Keto, E., Ball, R., Arens, J., Jernigan, G., & Meixner, M. 1992, ApJ, 389, 223

Kotilainen, J. K., Ward, M. J., Boisson, C., DePoy, D. L., Bryant, 1,. N.., & Smith, M. G. 1992, MNRAS, 256, 125

Krolik, J. }1., & Begelman, M. C. 1986, ApJ, 308, 1,55

Krolik, J. }1., & Begelman, M. C. 1988, ApJ, 329, 702

Matsuda, q'., Inoue, M., Sawada, K., Shims, E., & Wakamatsu, K. 1987, MNRAS, 229, 295

Mathis, J. S., 1990, ARA&A, 28, 37

Meixner, M., Puchalsky, R., Blitz, L., Wright, M. C. H., & Heckman, T. M. 1990, ApJ, 354, 158

Morris, S. I,., & Ward, M. J. 1988, MNRAS, 230, 639

Osterbrock, D. E., Tran, H. D., & Veilleux, S. 1992, ApJ, 389, 196

Planesas. 1'., Scoville, N., & Myers, S. '1'. 1991, ApJ, 369, 364

Puget, J. I,., & Luget, A. 1989, A&AS, 27, 161

Roberts, W. W. Jr., Huntley, J. K., & van Albada, G. D. 1979, ApJ, 233, 67

Roche, P. F., Aitken, D. K., Smith, C. 11., & Ward, M. J. 1991, MNRAS, 248,606

Scoville, N. Z., Matthews, K., Carico, D. P., & Sanders, D. 11.1988, ApJ, 327, 1,61

Sellgren, K. 1981, ApJ, 245, 138

Shlosman, I., Frank, J., & Begelman, M. C. 1989, Nature, 33845

Simkin, S., Su, H., & Schwarz, M. P. 1980, ApJ, 237,404

Schwarz, M. P. 1984, MNRAS, 209,93

Soifer, B. T., Sanders, D. B., Madore, B. F., Neugebauer, G., Danielson, G. E., Elias, J. H., Lonsdale, C. J., and Rice, W. 1,.1987, ApJ, 320, 238

Soifer, B. T., Russell, R., & Merrill, K. M. 1976, ApJ, 210,334

Telesco, C. M., Becklin, E. E., Wynn-Williams, C. G., & Harper, D. A. 1984, ApJ, 282,427

van Buren, 1). & Greenhouse, M. A. 1993, ApJ, in press.

Voit, G. M. 1992, MNRAS, 258, 841

Wilson, A. S., Helfer, T. T., Haniff, C, A., & Ward, M. J. 1991, ApJ, 381, 79

Wright, G. S., Joseph, R. D., Robertson, N. A., James, P. A., & Meikle, W, P. S. 1988, MNRAS, 233, 1

Wynn-Williams, C. G., & Becklin, E. E. 1985, ApJ, 290, 108

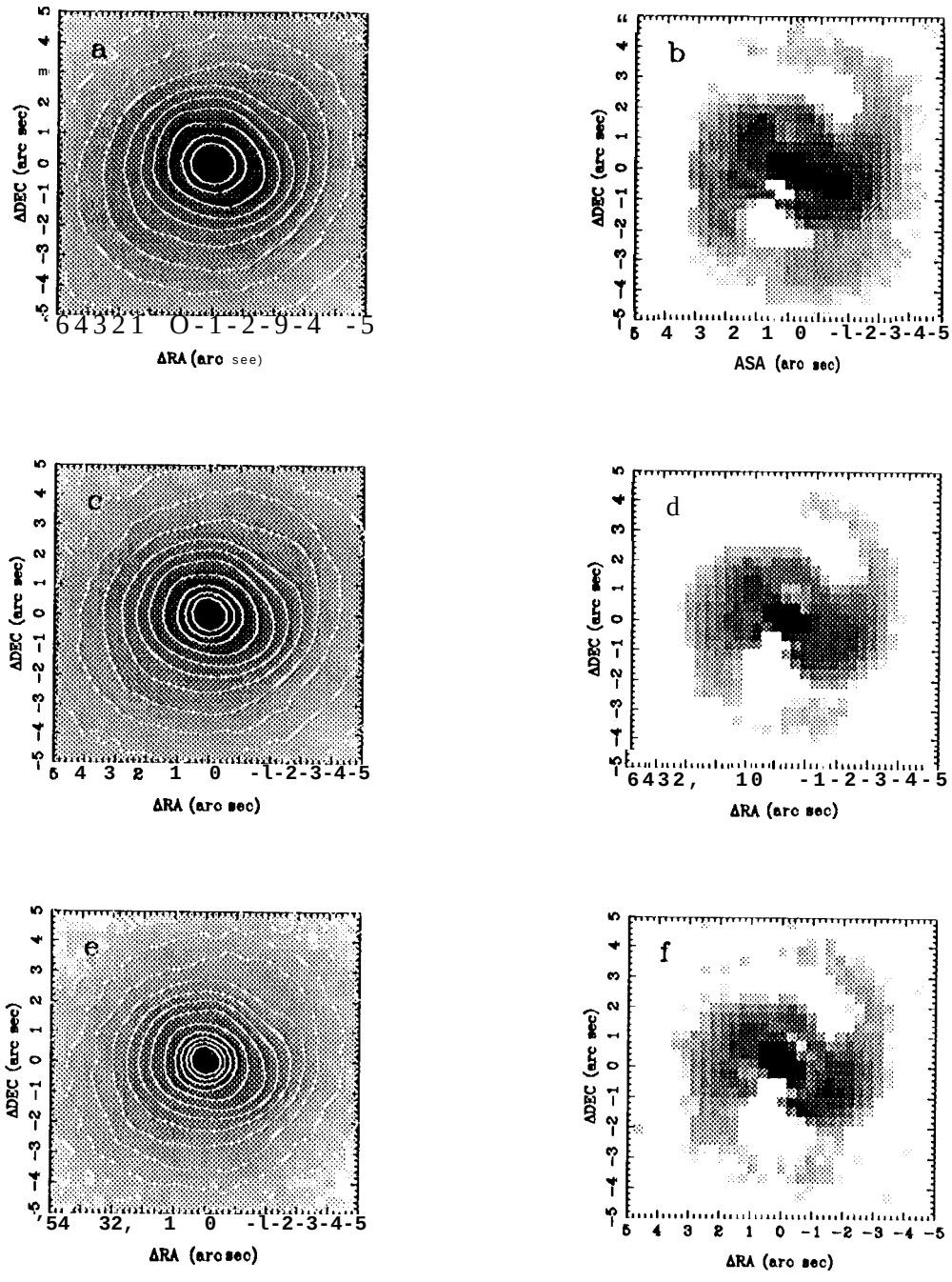

Fig. 1.- Direct and residual broad- band images of NGC 7469. Panels a, c, & e are gray-scale/contour overlays of *direct* J, 11, & K images, respectively; the contours arc drawn with a logarithmic interval, Panels b, d & f are gray-scales of *residual* images after subtraction of best-fit elliptical isophote models at J, 11, & K. Details of the ellipse fitting are described in the text.

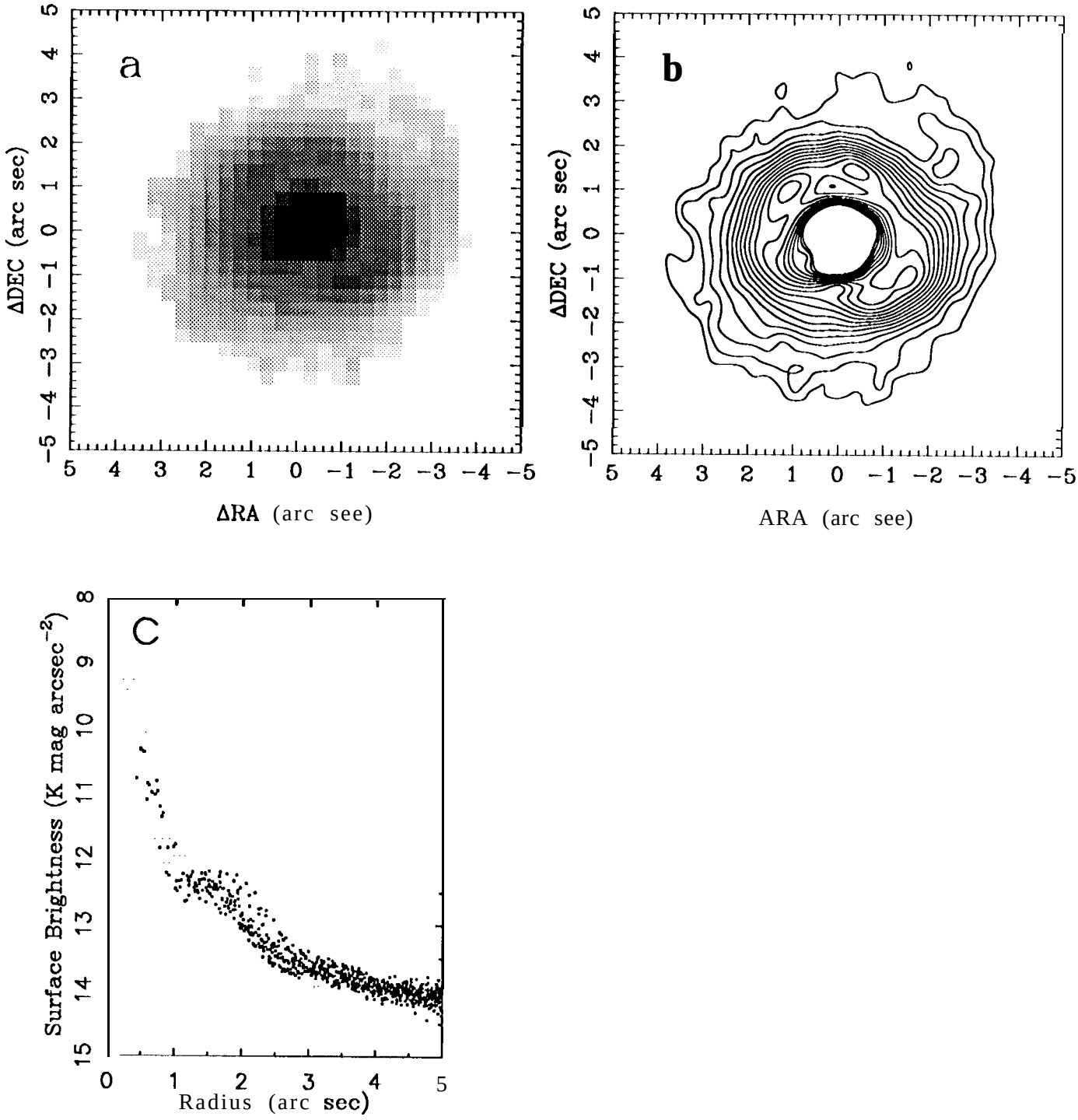

Fig. 2.- The direct K-band image after Richardson-Lucy restoration (FWHM=0.″65); (a) gray-scale; (b) logarithmic contours; (c) radial profile plot.

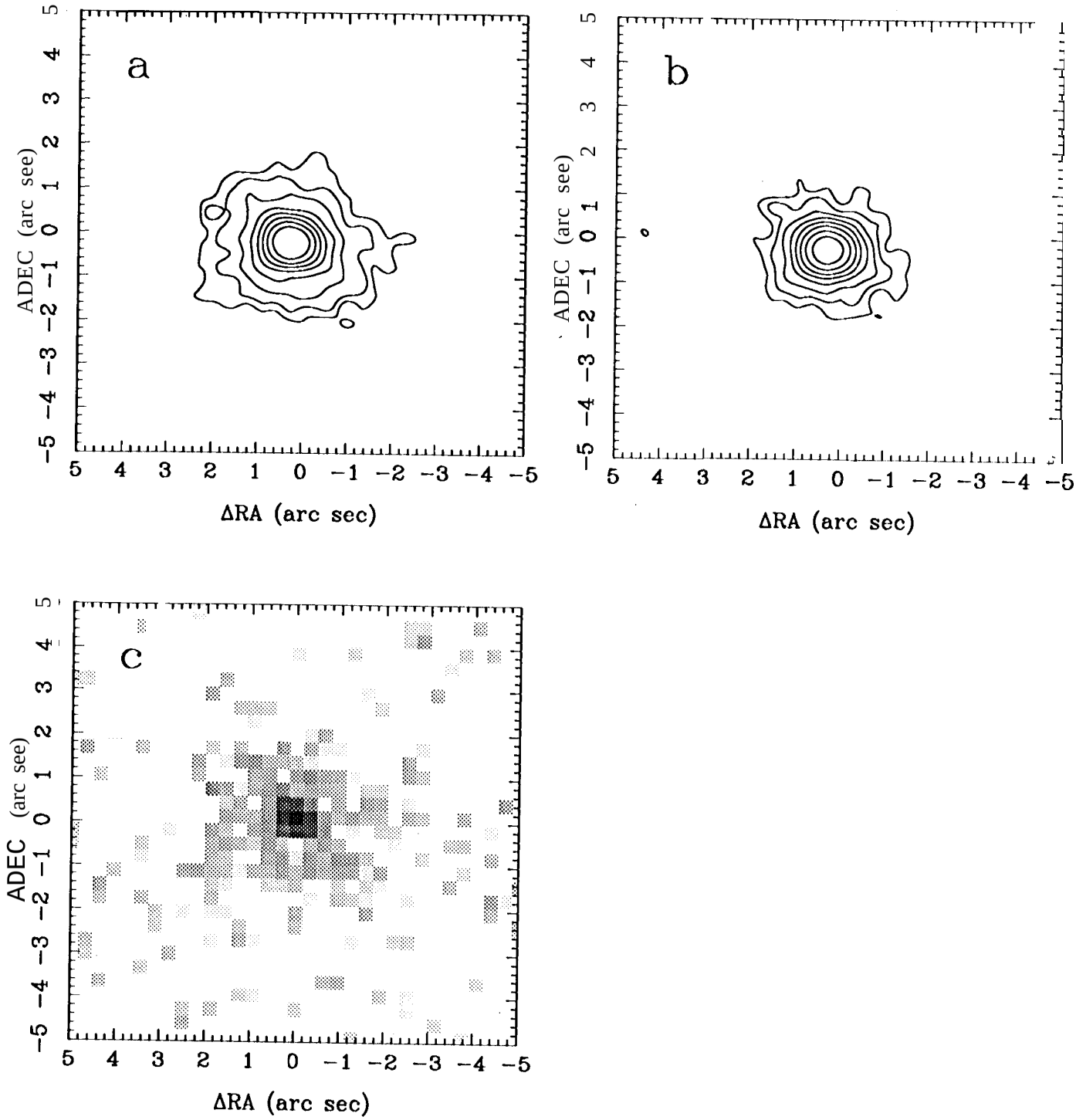

Fig. 3.– CVF ($\Delta\lambda/\lambda \sim 1.5\%$) images of NGC 7469. (a) ON the wavelength of the redshifted 3.3 μm PAH feature (average of 3.33 μm and 3.42 μm); (b) adjacent continuum OFF the PAH feature (3.20 μm); (c) ON minus OFF, continuum-subtracted 3.3 μm PAH image. The contours in panels (a) and (b) are plotted at the same intensity levels.

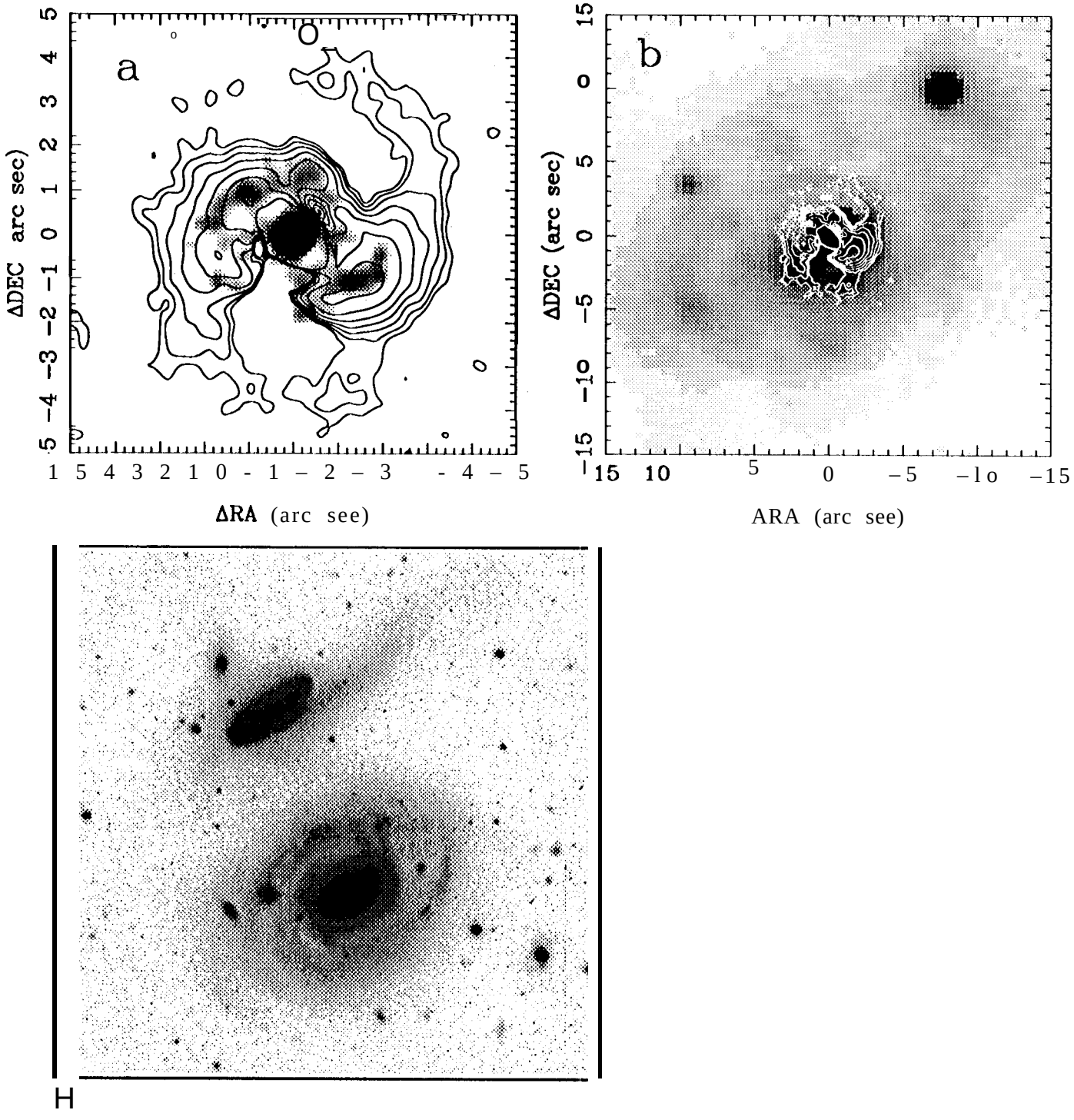

Fig. 4---- Illustration of the spiral structure at different spatial scales in NGC 7469; (a) contour diagram of the residual K-band image (also shown as a gray-scale in Fig. 1 f) superposed on a gray-scale of the 6 cm VLA image from Wilson et al. (1991); (b) contour diagram of the residual K-band image superposed on a gray-scale of a residual R-band image after subtraction of a smooth mode]; (c) gray-scale of a direct R-band image (the scale bar at the bottom left represents 10").